

# Application of antimonide lasers for gas sensing in the 3–4- $\mu\text{m}$ range

Peter Werle and Andrei Popov

Antimonide semiconductor laser devices designed for continuous-wave emission in the 3–4- $\mu\text{m}$  spectral range have been investigated with respect to spectroscopic applications. Representative data on the mode structure, output power, noise characteristics, far-field pattern, and modulation response are presented. Selected laser devices have been applied for methane ( $\text{CH}_4$ ) and formaldehyde ( $\text{HCHO}$ ) measurements by use of a high-frequency modulated diode laser spectrometer. From an Allan variance analysis of experimental data a detection limit for  $\text{HCHO}$  of 120 pptv (where 1 pptv =  $10^{-12}$  volume mixing ratio) with a 40-s integration time and for  $\text{CH}_4$  of 2 ppbv (where 1 ppbv =  $10^{-9}$  volume mixing ratio) with 20-s integration time were determined. The results show that, for selected gases, InAsSb lasers can be an alternative to lead-salt diode lasers. © 1999 Optical Society of America

*OCIS codes:* 300.6260, 300.6340, 300.6380, 010.1120, 140.2020, 140.3070.

## 1. Introduction

The reasons for limiting a widespread application of tunable diode laser absorption spectroscopy (TDLAS) in industrial process control are found in the relative complexity of current instrumentation and from the lack of high-quality, high-power diode lasers for many spectral regions of interest.<sup>1</sup> GaAs and InP lasers are widely commercially available. These diode lasers, made from the III–V group of semiconductor materials, emit at red and near-infrared (NIR) wavelengths from  $\sim 0.63$  to  $1.55 \mu\text{m}$ , including the GaAs/AlGaAs 0.78- and  $0.83\text{-}\mu\text{m}$  lasers used, for example, in compact-disk players. The technology of NIR 1.3- and  $1.55\text{-}\mu\text{m}$  InGaAsP/InP diode lasers developed for fiber-optic communication can be extended to the fabrication of lasers that emit anywhere in the wavelength interval of  $\sim 1.2\text{--}2 \mu\text{m}$ . A drawback of NIR diodes is that only a limited number of molecular species have absorption features in the spectral region covered by these lasers. Further-

more, the NIR absorptions are overtone or combination bands that are typically one to several orders of magnitude weaker than the IR fundamental band, but many molecules of interest have NIR absorption bands that are strong enough for detection at parts in  $10^6$  and, in some cases, even parts in  $10^9$  levels.<sup>2,3</sup>

Lead-salt diode lasers, made from IV–VI semiconductor materials, operate in the 3–30- $\mu\text{m}$  spectral region, and therefore they cover the IR fundamental band with strong absorptions for most atmospheric trace gases. They are used almost exclusively for spectroscopic applications. Because IV–VI lasers and their associated detectors operate at cryogenic temperatures, they are more expensive and more cumbersome to use than III–V devices. In trace-gas-monitoring applications, lead-salt laser instruments have routinely achieved ppbv levels (1 ppbv =  $10^{-9}$  volume mixing ratio) and in some cases even pptv (1 pptv =  $10^{-12}$  volume mixing ratio) detection levels of a number of important molecular species.<sup>4</sup> When comparing detection sensitivities, one has to keep in mind that sensitivities in real field applications will likely be less than those generated in the laboratory because of vibration and temperature and humidity excursions, among other factors.

The link between the NIR lasers and the mid-IR lead-salt diode lasers are antimonide-containing compounds such as AlGaAsSb, InGaAsSb, and InAsSbP, which allow the extension of NIR lasers to wavelengths longer than  $1.8 \mu\text{m}$  for the III–V group of semiconductor materials.<sup>3</sup> Room-temperature lasing from 2 to  $2.4 \mu\text{m}$  has been reported from simple

---

When this work was performed, P. Werle was with the Fraunhofer Institut, Kreuzackbahnstrasse 19, 82467 Garmisch-Partenkirchen, Germany, and A. Popov was with the Ioffe Physico Technical Institute, 194021 St. Petersburg, Russia. A. Popov is now with the Fachbereich Physik, AG Integrierte Optoelektronik, Universität Kaiserslautern, 67653 Kaiserslautern, Germany. The e-mail address for P. Werle is werle@ifu.fhg.de.

Received 17 June 1998; revised manuscript received 27 August 1998.

0003-6935/99/091494-08\$15.00/0

© 1999 Optical Society of America

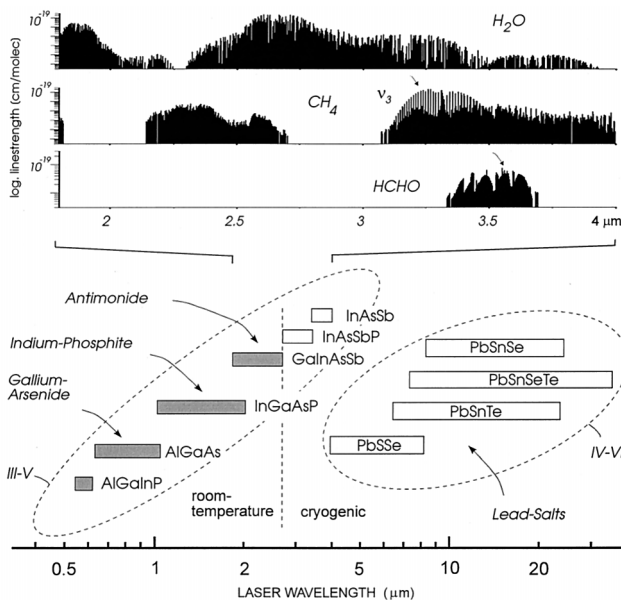


Fig. 1. Coverage of the spectral range from the visible to the mid-IR by tunable diode lasers of different material systems. For the antimonide lasers in the 1.8–4- $\mu\text{m}$  range, absorption bands for HCHO and  $\text{CH}_4$  are plotted together with the absorption band for water vapor.

double-heterostructure antimonide diode lasers.<sup>5</sup> As the wavelength increases up to 3.7  $\mu\text{m}$ , the maximum operating temperature decreases as a result of increasing optical and electrical losses. Recently III–V devices based on InAsSb/InAsSbP manufactured at the Ioffe Physico Technical Institute (St. Petersburg, Russia) have been investigated with respect to spectroscopic applications.<sup>6–9</sup> These double-heterostructure devices were grown by liquid-phase epitaxy on an InAs substrate and covered the spectral range from 3 to 4  $\mu\text{m}$  at liquid-nitrogen ( $\text{LN}_2$ ) temperatures. In this paper a detailed characterization shows that these devices are well suited for the detection of HCHO at 3.57  $\mu\text{m}$  and  $\text{CH}_4$  at 3.25  $\mu\text{m}$  and that the single-mode power of more than 1 mW is especially attractive for spectroscopic trace-gas monitoring with optical multipass cells.

Figure 1 gives an overview of different types of semiconductor laser, from the visible to the IR regions, together with some absorption bands of atmospheric HCHO and  $\text{CH}_4$ .<sup>10</sup> Various systems have been developed for the detection of HCHO. They are based mainly on fluorescence techniques and diode laser absorption spectroscopy.<sup>11,12</sup> Another promising technique for compact, room-temperature solid-state sensors for HCHO in the 3–5- $\mu\text{m}$  spectroscopic region is based on difference-frequency generation.<sup>13</sup> Fast chemical sensors for atmospheric-greenhouse-gas monitoring are important for applications in global warming control.<sup>14</sup>  $\text{CH}_4$  absorbs thermal radiation approximately 30 times more efficiently (per unit mass) than  $\text{CO}_2$  does. Its concentration increases  $\sim 20$  ppbv/year, produced by natural-gas releases, fuel combustion,

biomass burning, and rice paddy cultivation. TD-LAS monitoring of  $\text{CH}_4$  has been done with a lead-salt diode laser by use of the two strong fundamental absorption bands located near 7.7 ( $\nu_4$ ) by Verma *et al.*<sup>15</sup> and near 3.3  $\mu\text{m}$  ( $\nu_3$ ) by Edwards *et al.*,<sup>16</sup> as well as with weaker overtone bands at 1.3  $\mu\text{m}$  ( $\nu_2 + 2\nu_3$ ) by Rooth and Kema<sup>17</sup> and at 1.65  $\mu\text{m}$  ( $2\nu_3$ ) by Hovde *et al.*<sup>18</sup> So far, all mid-IR TDLAS instruments are based on lead-salt lasers as the source of radiation, but it is still a problem to fabricate reliable lasers for 3.3  $\mu\text{m}$ . Antimonide diode lasers, which can operate at up to 4- $\mu\text{m}$  wavelengths, are expected to obtain higher cw output powers since their thermal conductivity and material stability under a strong dc injection current are superior compared with those of lead salts.

## 2. Laser Diodes and Experimental Setup

The antimonide lasers under investigation are based on an InAsSb/InAsSbP double heterostructure grown on an InAs (100) substrate. A 0.5–1.0- $\mu\text{m}$ -thick active layer is enclosed between two 3- $\mu\text{m}$ -thick InAsSbP claddings. The composition of the active layer corresponds to a lasing wavelength of 3–4  $\mu\text{m}$  at 77 K. For a more detailed description of the antimonide lasers under investigation, the reader is referred to Refs. 5–9. The double-channel mesa laser with a 300- $\mu\text{m}$ -length Fabry–Perot cavity and uncoated facets is mounted on a copper heat sink [Fig. 2(a)] and installed in a Dewar [Fig. 2(b)] for cw operation above  $\text{LN}_2$  temperatures. For high-FM applications and investigations of the wideband noise characteristics, a bias T was mounted close to the laser for impedance matching. In general, we found that thermal cycling was not critical and if the laser was cycled several times the operating points remained almost the same. This was different if the laser had been dismantled and remounted in the same or in another Dewar. Then thermal coupling might have changed and previously measured mode maps would no longer be valid. Therefore the laser stayed in the same Dewar for a detailed spectral characterization in the laser test setup and for the subsequent application measurements in the spectrometer described below.

To investigate the suitability of the antimonide lasers for trace-gas measurements, a laser test setup was used, that allowed recording of laser optical power, mode structure, and wideband noise characteristics over a broad range of injection currents and junction temperatures.<sup>19</sup> The schematic layout of the setup is shown in Fig. 2(c). The laser was mounted in a  $\text{LN}_2$ -cooled Dewar (Laser Photonics, L5739), was temperature and current stabilized over the range from 77 to 120 K and between 0.300 mA with an ILX Lightwave LDC 3742 power supply, and was additionally mounted on an *xyz* stage for focus alignment. An off-axis parabolic mirror with a 25-mm diameter was used to collimate the laser output beam. Electrically actuated mirrors were used to pass the beam through the various elements. The laser beam could be directed on a calibrated pyroelec-

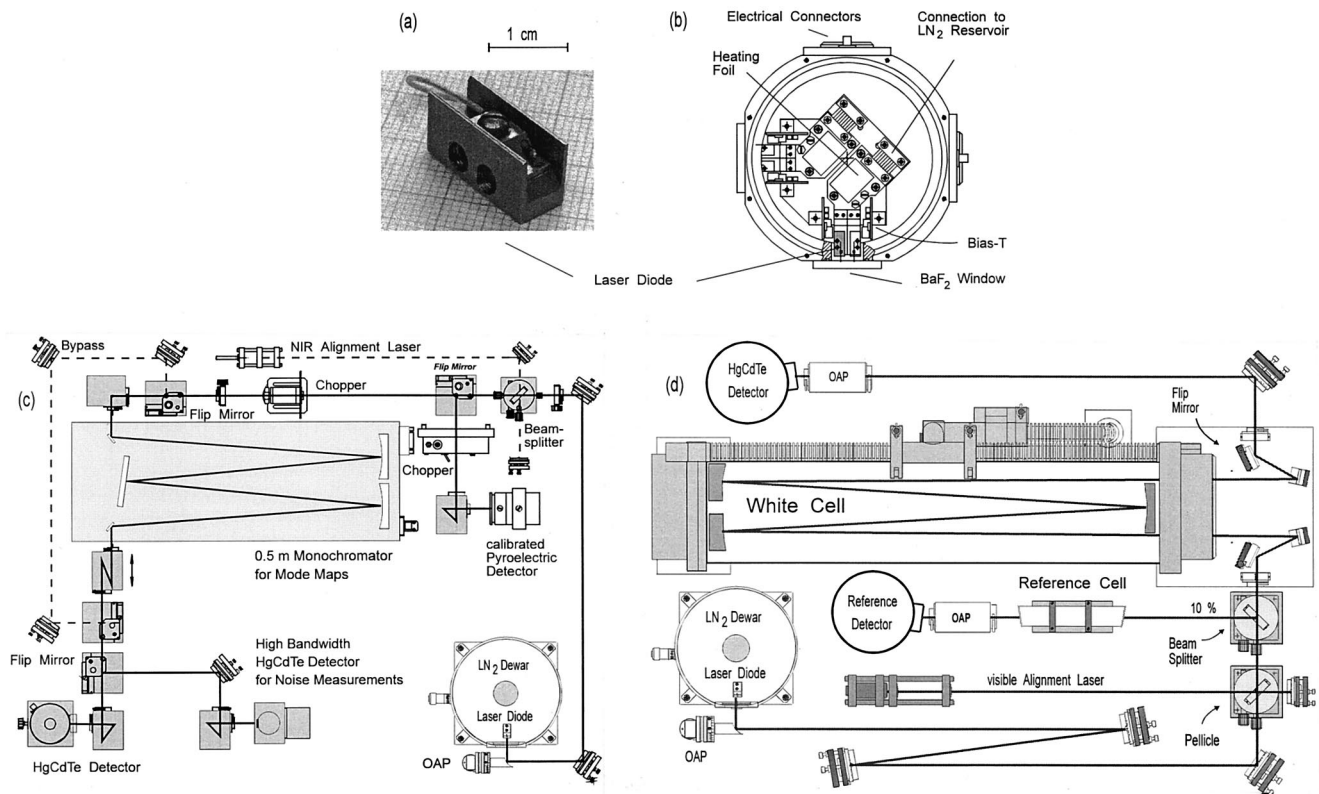


Fig. 2. (a) InAsSb laser in a standard housing, mounted close to the (b) bias T in the Dewar for recording (c) mode maps, output power, wideband noise characteristics, and far-field pattern in a test setup; (d) for analytical measurements the Dewar is moved to the spectrometer. OAP's, off-axis parabolic mirrors.

tric powermeter (Laser Precision, RS 5900) or steered through a 0.5-m monochromator (Digikröm 480). A bypass was implemented to allow the measurement of the unfiltered beam. Another mirror was used to switch between two modes of operation: either a 200-MHz-bandwidth HgCdTe detector (SAT), followed by a low-noise preamplifier (SAT IR 500) and a high-frequency spectrum analyzer (Marconi SA 2383) were used for noise measurements, or a chopper (SR 540) and a HgCdTe detector (Polytec HCT 70) combined with a lock-in amplifier (SR 530) were selected for relative power measurements while the monochromator was scanning the mode structure. A He-Ne laser was coupled into the system by a removable beam splitter to prealign the whole system. A problem did arise from the fact that the InAsSb lasers under investigation had a much larger half-width emittance angle as the previously used lead-salt lasers. Because of the limited size of the off-axis parabolic mirror (25-mm diameter at 32-mm focal length), a separate external optical output-power measurement with a 25-mm BaF<sub>2</sub> lens was made to get the full emitted power on the meter. The laser field patterns were recorded by a pyroelectric camera placed directly in front of the laser.

The mid-IR TDLAS system,<sup>20</sup> which has been used for the spectroscopic detection of CH<sub>4</sub> and HCHO based on antimonide lasers is shown in Fig. 2(d). The optical setup is mounted on a 1 m × 0.6 m optical

breadboard. The antimonide diode laser is housed in the same LN<sub>2</sub>-cooled Dewar, which was used for the spectral characterization in the laser test setup above. To accommodate a possible deviation angle between the cone of laser emission and the laser mount axis, the LN<sub>2</sub> Dewar is mounted on an *xyz* stage alignable to within ±30°. The beam from the TDL is first collimated by an off-axis paraboloid and then directed by a sequence of mirrors through the sample cell and onto a LN<sub>2</sub>-cooled HgCdTe photovoltaic detector. A visible 670-nm laser beam is combined by means of a pellicle beam splitter with the invisible IR beam to assist in alignment. Because of low transmission in the IR, the pellicle beam splitter is kinematically mounted and can be removed during the trace-gas measurements. Typical line strengths are such that an atmospheric concentration of 1 ppbv produces an absorption of only 1 part in 10<sup>7</sup> over a 10-cm path length. Conventional absorption spectroscopy techniques will clearly not be able to measure such small absorptions. With TDLAS this problem is overcome by use of a multipass cell with path lengths of 100 m or even more. Such cells achieve the long path by using mirrors to fold the optical path, giving typically 100 passes of a 1-m base-length cell. A commercial White cell module (Mütek MDS 1600) with a base length of 62.5 cm and an adjustable path length of up to 100 m is shown together with the focusing optics in Fig. 2(d).

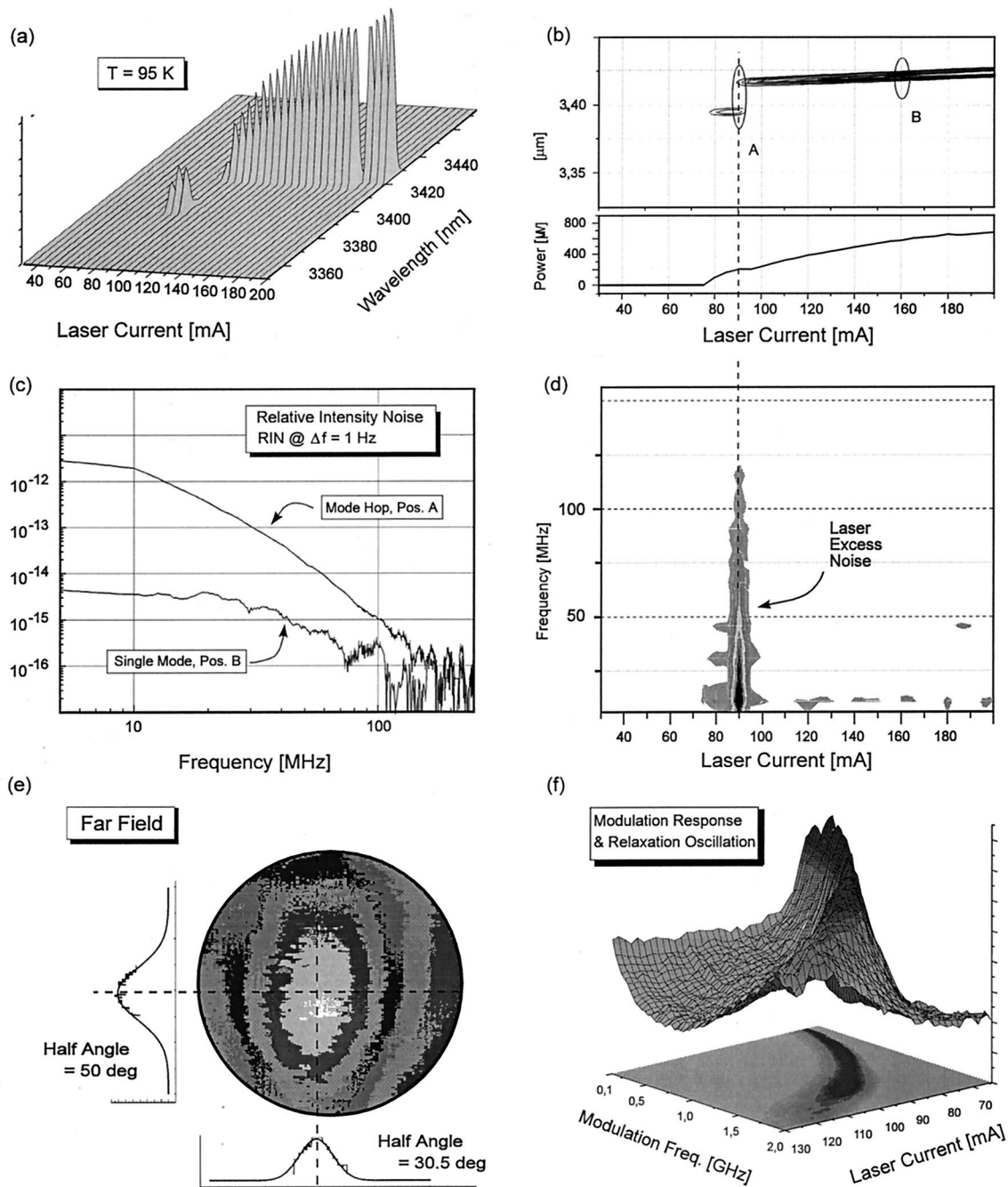


Fig. 3. Characteristic results obtained from the laser test setup: (a) mode map, (b) power measurement, (c) relative intensity noise, (d) laser excess noise at a mode-hop position, (e) far-field pattern, (f) the modulation response.

### 3. Experimental Results

Different InAsSb lasers were investigated in detail and preselected for ambient measurements by use of the test setup described in Section 2. Figure 3 summarizes some typical results. For the laser shown here, we observed a mode hop at 90 mA immediately above threshold of  $\sim 80$  mA at 95 K. Then a dominant single-mode emission, starting from 90 up to 200 mA was observed [Fig. 3(b)] together with an output power of up to  $700 \mu\text{W}$ . The noise measurements in Figs. 3(c) and 3(d) illustrate the superior noise characteristics in the single-mode regime (B)

relative to the simultaneous emission of two modes near the mode-hop position (A). These results are the same as those for lead-salt diode lasers.<sup>1,19</sup> The far-field distribution [Fig. 3(e)] is especially important for high-FM application because maximum beam intensity has to be focused on a small-area detector element. The modulation response displayed in Fig. 3(f) illustrates that relaxation oscillations occur well beyond the modulation frequencies used for high-FM techniques.<sup>8</sup> The results summarized in these plots are representative for most antimonide lasers we have investigated so far. In

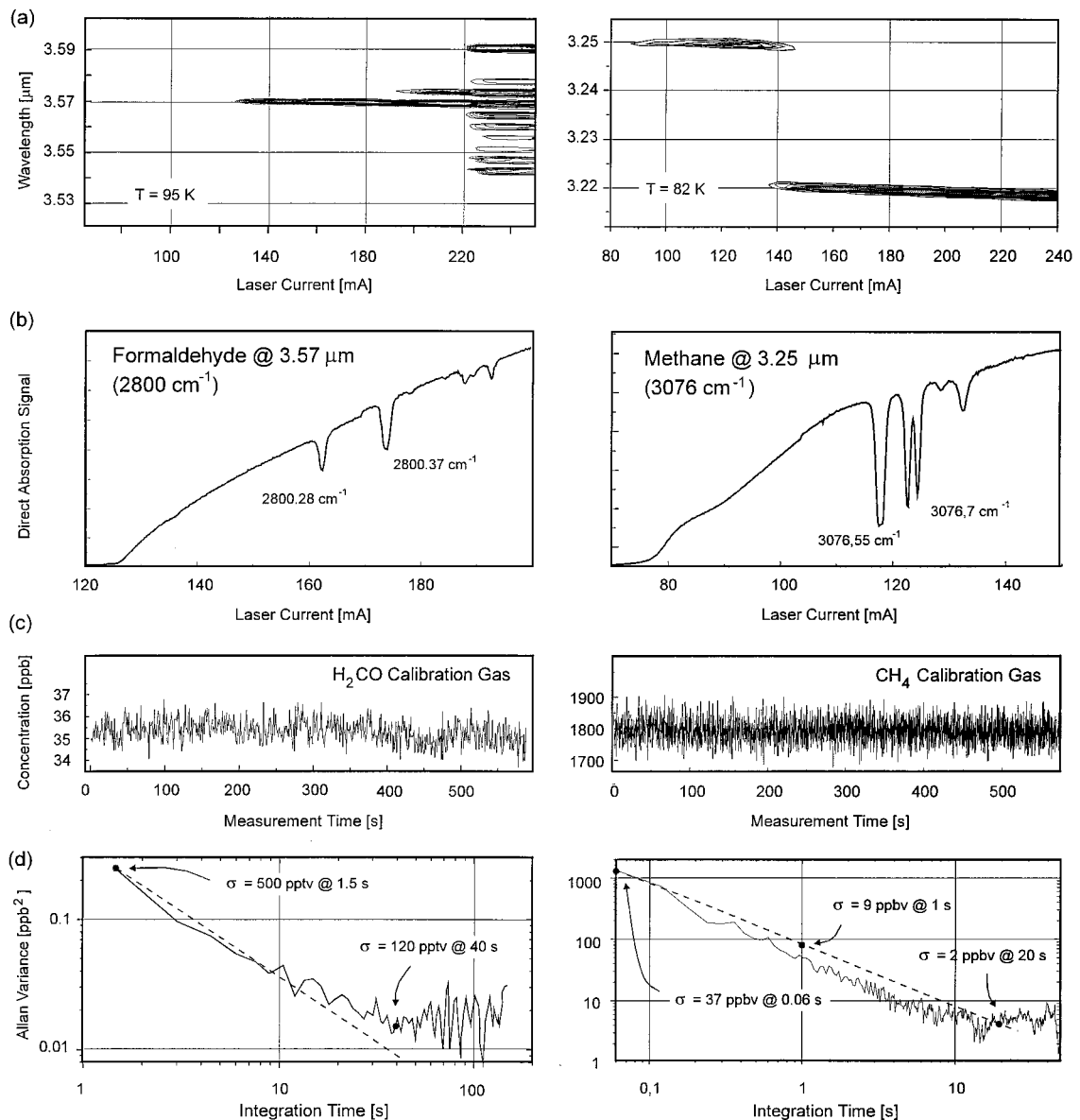


Fig. 4. Characteristic results obtained from the spectrometer for HCHO (left-hand side) and CH<sub>4</sub> (right-hand side): (a) mode map, (b) direct absorption signals during scan, (c) time-series concentration data, (d) Allan plots<sup>19</sup> to characterize system stability. The dashed lines indicate the expected noise reduction for white noise.

general we found that there are no significant discrepancies in performance compared with that of lead-salt diode lasers, besides the fact that the observed single-mode emission power is up to 1 order of magnitude higher for the antimonide lasers under investigation.

For trace-gas-sensing applications, two lasers have been selected: one for HCHO emitting at 3.57 μm (2800.2 cm<sup>-1</sup>) and one for CH<sub>4</sub> operating at 3.25 μm (3076.5 cm<sup>-1</sup>). Characteristic results obtained from the test setup and the spectrometer are displayed in Fig. 4 for HCHO (left-hand side) and CH<sub>4</sub> (right-hand side); Fig. 4 shows the laser mode map [Fig. 4(a)], the direct absorption signals during the injection current scan [Fig. 4(b)], time-series concentration data obtained from FM signals [Fig. 4(c)], and the corre-

sponding Allan Plots to characterize the system stability [Fig. 4(d)].

First we briefly discuss the HCHO measurement. During the investigations of Section 2 with the test setup the mode structure was recorded for different temperatures. During this experiment the temperature of the laser was set to 95 K, which resulted in lasing at 3.57 μm with 400-μW optical power [Fig. 4(a)]. The laser tuning rates at 95 K were typically below 300 MHz/mA. In this spectral region a series of strong absorption lines suitable for the detection of HCHO at ambient concentrations was found when a reference absorption cell with a high HCHO concentration was placed in the laser beam [Fig. 4(b)]. The White cell in the spectrometer was set to a 30-m absorption path, and the pressure inside the cell was

set to 30 mbars. The laser was repetitively tuned over an absorption line at  $2800.28\text{ cm}^{-1}$  (line strength  $S = 4.4 \times 10^{-20}\text{ cm/molec}$ ) and modulated at 120 MHz. Because of the application of the single-tone high-FM technique, the absolute value of the direct absorption signal was lost and therefore a calibration system, which provided zero air (air devoid of the target gas) and a constant amount of HCHO calibration gas, was added to the setup. For the determination of the ambient-gas concentration, calibration gas, zero air (background), and ambient-air spectra were recorded in the long-path absorption cell. After the subtraction of the zero-air spectrum from the calibration and the ambient spectra, the concentration was calculated by a multilinear regression analysis.<sup>21</sup> This baseline cancellation reduces the influence of baseline features caused by the non-linearity in the emitted laser power versus injection current or because of the presence of fringes in the optical system. However, baseline cancellation works only if the baseline distortion is stable over time. Therefore we carefully analyzed the system stability in terms of the Allan variance.<sup>20</sup> Figure 4(c) shows time-series data of calibration gas recorded over a period of 10 min. From the corresponding Allan plot [Fig. 4(d)] the optimum averaging time can be derived to be of the order of 40 s. This time defines the maximum interval for a complete measurement cycle: sample measurement, background measurement, and gas-exchange time. If a measurement cycle exceeds this experimentally determined time, the data are no longer reliable. The measured standard deviation of the HCHO measurement was 500 pptv at a 1.5-s integration time and a 6.25-Hz bandwidth. In terms of noise-equivalent optical absorption, this translates into  $1 \times 10^{-6}$  at a 1-Hz bandwidth. For the ultimate detection limit for the given experimental conditions we obtained 120 pptv at a 40-s integration time. It should be noted that this precision has been actually calculated from the measured concentrations and is not an extrapolation.<sup>20</sup> For integration times longer than 40 s the system stability is insufficient, and a  $1/f$ -type noise dominates the measurements. This noise contribution has been attributed to turbulent fluctuations in the multipass cell. The fluctuations are due to the expansion of the ambient air into the cell, where the pressure is regulated to 30 mbars. We have recently shown that the spectra of the density fluctuations are of the  $1/f$ -type.<sup>22</sup> These refractive-index fluctuations translate into phase fluctuations, and averaging of  $1/f$ -type noise will no longer increase precision.<sup>20,22</sup> The main limitation therefore comes from the turbulent gas flow in the cell as well as from the presence of weak fringes in the system. However, the results of these measurements are well in line with  $\text{NO}_2$  measurements made with a lead-salt diode laser in the same system near  $6\text{ }\mu\text{m}$ .<sup>20</sup> This application of antimonide lasers for HCHO measurements at ambient concentration levels clearly demonstrated that they can compete with lead-salt lasers.

In a second series of experiments we investigated the performance of the antimonide laser selected for  $\text{CH}_4$  measurements. The mode map obtained at 82 K is displayed in Fig. 4(a) (right-hand side). The threshold current was  $\sim 80\text{ mA}$  dc and the laser output power was in the range 0.2–0.6 mW/facet. The laser showed single-mode operation over a broad temperature and current range. Lasing at  $3.25\text{ }\mu\text{m}$  ( $3076\text{ cm}^{-1}$ ) was observed close to the threshold. The laser tuning rates at 82 K were typically  $\sim 300\text{ MHz/mA}$  (at lower temperatures they are higher by a factor of 2–3). This behavior was attractive for field measurements because the noise of the current controller ( $\sim 10\text{ }\mu\text{A}$ ) will not limit the required frequency stability. To set the optimal condition for laser driving we made tests with a single-pass absorption cell filled with  $\text{CH}_4$  at a high concentration [Fig. 4(b)]. The measured absorption spectra were compared with those given in the HITRAN database to identify the strongest absorption lines that would not interfere with other gases. Only one group of strong  $\text{CH}_4$  lines could be detected at  $3076.5\text{ cm}^{-1}$  ( $3.25\text{ }\mu\text{m}$ ), slightly above threshold at low current values, where the emitted laser power unfortunately was below  $200\text{ }\mu\text{W}$ . With the mode at  $3105\text{ cm}^{-1}$  ( $3.22\text{ }\mu\text{m}$ ) providing higher laser power, only absorption lines that were weaker by 2 orders of magnitude could be accessed, and therefore we selected an absorption line with a line strength  $S = 1.2 \times 10^{-19}\text{ cm/molec}$  at  $3076.56\text{ cm}^{-1}$  for the  $\text{CH}_4$  measurements.

The FM TDLAS instrument was set to high-speed mode, which allows fast measurements with a repetition rate of 10 Hz, an integration time of 0.06 s, and a bandwidth of 83 Hz. This spectrometer mode is used to determine the exchange of trace gases between biosphere and atmosphere with the eddy correlation method for emission and deposition measurements.<sup>15,16</sup> This technique correlates the vertical wind and the trace-gas concentration fluctuations. For this type of measurement the concentration fluctuation must be recorded at  $\sim 10\text{ Hz}$  to determine the trace-gas flux correctly. During the modification of the system for eddy correlation measurements, the White cell was replaced by a Herriott cell with a fixed path length of 100 m (Aerodyne Research). For reliable measurements of  $\text{CH}_4$  fluxes, the precision of the measured concentration fluctuation should be better than  $5 \times 10^{-3}$ . For typical ambient  $\text{CH}_4$  concentrations of 1800 ppbv, this corresponds to a detection limit of  $\sim 10\text{ ppbv}$  in 0.1-s averaging time or 3.3 ppbv in 1 s. This value was obtained previously with the same spectrometer with a lead-salt diode laser at  $7.8\text{ }\mu\text{m}$  and a  $\text{CH}_4$  absorption line that was weaker by a factor of  $\sim 2$ –4, compared with the strongest one in the  $\nu_3$  band near  $3.3\text{ }\mu\text{m}$ . The reference channel consisted of a cell filled with a high  $\text{CH}_4$  concentration and produced a strong absorption signal for line locking. The high-resolution time-series data from the measurement cell (flushed with  $\text{CH}_4$  calibration gas of 1.8 ppmv at 30 mbar) are displayed in Fig. 4(c). Based on these

data, the performance of the spectrometer was again analyzed in terms of the Allan variance. With the selected laser a maximum integration time of  $\sim 20$  s can be derived. The standard deviation of the measured  $\text{CH}_4$  concentration was 37 ppbv for an integration time of 0.06 s, which translates into 9 ppb at 1 s. The Allan plot of Fig. 4(d) (right-hand side) gives even slightly better results for a 1-s integration time, and for the ultimate detection limit for the given experimental conditions we obtain  $\sim 2$  ppbv at a 20-s integration time. For longer integration times the system stability is insufficient and again a  $1/f$ -type noise dominates the measurements, as we discussed above in the context of the HCHO measurements.<sup>22</sup> In terms of optical absorption this performance is equivalent to  $2.7 \times 10^{-4}$  at a 1-Hz bandwidth.

If we compare this result with the above-stated 3.3 ppbv in 1 s for the lead-salt system, at least a factor of 3 is missing. Besides the already discussed turbulence and fringe problems, the measurements shown here suffer from the lack of laser power available on the detector. In principle, high-FM spectroscopy is capable of quantum-noise-limited performance. The signal-to-noise ratio under quantum-limited conditions scales with the square root of the power available on the detector, and to obtain quantum-limited conditions, the laser power has to be high enough to make shot noise the dominating noise source.<sup>23</sup> We should keep in mind that the spectrometer has originally been designed for applications with lead-salt diode lasers and is optimized for the 5–10- $\mu\text{m}$  range. Therefore, for measurement applications of antimonide lasers, the HgCdTe detectors with a peak  $D^*$  at 10.6  $\mu\text{m}$  should be replaced by InSb (77-K) detectors, which are more suited for the 3–4- $\mu\text{m}$  spectral range under investigation. In addition, at 3.3  $\mu\text{m}$ , the reflectivity of the mirrors in the long path cell is reduced and only  $\sim 4$   $\mu\text{W}$  of the laser power reaches the photodetector. Taking into account (1) the lower mirror reflectivity that causes a reduced transmission of the optical system, (2) the low power of the laser, which has to be operated slightly above threshold, and (3) the lower spectral response of the HgCdTe detector in this spectral range, we find that the detection limit is comparable with that of lead-salt lasers.

#### 4. Summary and Conclusion

In summary, a series of InAs/InAsSbP double-heterostructure lasers was investigated with respect to spectroscopic applications. Therefore mode maps were recorded for different temperatures of the  $p$ - $n$ -junction. These measurements were completed by recording the wideband noise characteristics to determine the relative intensity noise at single-mode positions and in the vicinity of mode hops. As stated above for lead-salt diode lasers,<sup>19</sup> the presence of spurious side modes dramatically increased the noise in the detection circuitry and therefore degraded the system performance. Additionally the far field was investigated to check the focusing quality, which can be obtained to optimize the power transmission of the

system. Investigations of the modulation response completed the picture and showed that relaxation oscillations occur well beyond the modulation frequencies normally applied in FM spectrometers.

Measurements of HCHO and  $\text{CH}_4$  with selected antimonide laser devices have been presented. From our first experiments we determined a detection limit for HCHO of 120 pptv with a 40-s integration time or  $(\alpha L)_{\min} = 10^{-6}$  at  $\Delta f = 1$  Hz, and for  $\text{CH}_4$  we obtained 2 ppbv with a 20-s integration time  $(\alpha L)_{\min} = 2.7 \times 10^{-4}$  at  $\Delta f = 1$  Hz. The achievable detection limits scale with the integration time, as illustrated by the corresponding Allan plots. As the spectrometer is usually operated with lead-salt diode lasers, it has not been optimized for the spectral range between 3 and 4  $\mu\text{m}$ : The spectral response of the HgCdTe detectors degrades near 3  $\mu\text{m}$ , and InSb detectors should be used instead. With an optimized system with respect to optical power transmission and an antimonide laser that emits at the right wavelength at higher injection currents, the potential of the increased line strength in the  $\nu_3$  band of  $\text{CH}_4$  should be feasible with antimonide lasers. Furthermore, we expect substantial improvement in system performance by applying double-modulation schemes for the suppression of fluctuations and baseline drifts, which currently limit, in most cases, the sensitivity.<sup>24</sup>

From the limited number of antimonide lasers we have investigated up to now, we can say that the observed single-mode emission power was up to 1 order of magnitude higher than that for lead-salt diode lasers. This is attractive, especially for high-FM applications, and might lead to an improved system performance in the future. Therefore antimonide lasers can offer operational benefits compared with those of lead-salt diode lasers while still maintaining the high sensitivity that is the result of probing fundamental rovibrational absorption transitions. The antimonide lasers still need a cryogenic Dewar; these lasers operate in single longitudinal modes over limited regions since they are Fabry-Perot devices, and they are not easily fiber coupled, so the sensor still remains complex.

Since 1996 lead salts and antimonides have been facing competition from a relatively new direction. Until recently all semiconductor lasers, regardless of their operating wavelength, relied on direct band-to-band transitions in bulk material or analogous transitions in type I quantum wells. Rapid progress has been reported in mid-IR lasers based on new types of transitions. The most notable examples of these types of lasers are the quantum-cascade lasers and type II quantum-well lasers. Quantum-cascade lasers operate on transitions within the conduction subbands of multiple quantum wells and have been pioneered by Bell Laboratories. Operation above room temperature was recently reported for the first time for quantum-cascade lasers emitting at 5  $\mu\text{m}$  in pulsed mode and up to  $T = 140$  K in cw operation.<sup>25</sup> The other new development is the type II quantum-well laser in GaInSb/InAs, which operates pulsed at

250 K at 3.2  $\mu\text{m}$ . While these new types of laser are still in the experimental stage, they appear to offer the prospect of more robust construction and higher-temperature operation than is possible with the materials that have been used up to this point.<sup>26</sup>

This study has been funded by the European Community under Copernicus contract CIPA-CT94-0158 and by a DAAD-NATO grant A97/52215 for Andrei Popov. We thank Victor Sherstnev for the preselection of lasers, Robert Mücke for his assistance in preparing the manuscript, and Bernd Jänker for his engineering support. The valuable suggestions of the reviewers to improve the manuscript are gratefully acknowledged.

## References

1. P. Werle, "A review of recent advances in semiconductor laser based trace gas analyzers," *Spectrochim. Acta A* **54**, 197–236 (1998) and references therein.
2. P. Werle, R. Mücke, F. D'Amato, and T. Lancia, "Near-infrared trace gas sensors based on room temperature diode-lasers," *Appl. Phys. B* **67**, 307–315 (1998).
3. R. U. Martinelli, R. J. Menna, P. K. York, D. Z. Gabuzov, H. Lee, J. Abeles, N. A. Morris, J. C. Conolly, S. Y. Narayan, J. S. Vermaak, G. H. Olsen, D. E. Cooper, C. B. Carlisle, and H. Riris, "Tunable single-frequency III–V semiconductor diode lasers with wavelengths from 0.76 to 2.7  $\mu\text{m}$ ," in *Application of Tunable Diode Lasers and Other Infrared Sources for Atmospheric Studies and Industrial Monitoring*, A. Fried, ed., Proc. SPIE **2834**, 2–16 (1996).
4. H. I. Schiff, G. I. Mackay, and J. Bechara, "The use of tunable diode laser absorption spectroscopy for atmospheric measurements," in *Air Monitoring by Spectroscopic Techniques*, M. W. Sigrist, ed., (Wiley, New York, 1994).
5. A. Popov, V. Sherstnev, Y. Yakovlev, R. Mücke, and P. Werle, "High power InAsSb/InAsSbP double heterostructure lasers for continuous wave operation at 3.6  $\mu\text{m}$ ," *Appl. Phys. Lett.* **68**, 2790–2792 (1996).
6. A. Popov, V. Sherstnev, Y. Yakovlev, R. Mücke, and P. Werle, "Single-frequency InAsSb lasers emitting at 3.4  $\mu\text{m}$ ," *Spectrochim. Acta A* **52**, 863–870 (1996).
7. A. Popov, A. Baranov, V. Sherstnev, Y. Yakovlev, B. Scheumann, R. Mücke, and P. Werle, "Investigation of the mode structure and noise characteristics of InAsSb/InAsSbP lasers with respect to spectroscopic applications," *Infrared Phys. Technol.* **37**, 117–121 (1996).
8. A. Popov, V. Sherstnev, Y. Yakovlev, R. Mücke, and P. Werle, "Relaxation oscillations in single-frequency InAsSb narrow band-gap lasers," *Appl. Phys. Lett.* **72**, 3428–3430 (1998).
9. A. Popov, V. Sherstnev, Y. Yakovlev, R. Mücke, and P. Werle, "Tuning and spectral performance of mid-infrared InAsSb lasers," in *Application of Tunable Diode Lasers and Other Infrared Sources for Atmospheric Studies and Industrial Monitoring*, A. Fried, ed., Proc. SPIE **2834**, 46–56 (1996).
10. L. S. Rothman, R. R. Gamache, R. H. Tipping, C. P. Rinsland, M. A. H. Smith, D. C. Brenner, V. Malathy Devi, J.-M. Flaud, C. Camy-Peyret, A. Perrin, A. Goldman, S. T. Massie, L. R. Brown, and R. A. Toth, "The HITRAN molecular databases editions of 1991 and 1992," *J. Quant. Spectrosc. Radiat. Transfer* **48**, 469–507 (1992).
11. A. Fried, S. Sewell, B. Henry, B. P. Wert, T. Gilpin, and J. Drummond, "Tunable diode laser absorption spectrometer for ground based measurements of formaldehyde," *J. Geophys. Res.* **102**, 6253–6266 (1997).
12. R. Kormann, K. Maurer, R. Mücke, F. Slemr, P. Werle, R. Zitzelsberger, U. Parchatka, T. Zenker, D. Trapp, and H. Fischer, "Application of two tunable diode laser spectrometers and other chemical sensors in an intercomparison of formaldehyde measurements," in *Proceedings of EUROTRAC Symposium '96* by P. M. Borrell *et al.*, eds. (Computational Mechanics, Southampton, England, 1996), pp. 715–719 (1996).
13. D. G. Lancaster, D. Richter, R. F. Curl, and F. K. Tittel, "Real-time measurements of trace gases using a compact difference-frequency-based sensor operating at 3.5  $\mu\text{m}$ ," *Appl. Phys. B* **67**, 339–345 (1998).
14. L. Newman, ed., *Measurement Challenges in Atmospheric Chemistry* (American Chemical Society, Washington, D.C., 1993).
15. S. B. Verma, F. G. Ullman, D. Billesbach, R. J. Clement, J. Kim, and E. S. Verry, "Eddy correlation measurements of methane flux in a northern peatland ecosystem," *Boundary-Layer Meteorol.* **58**, 289–304 (1992).
16. G. C. Edwards, H. H. Neumann, G. den Hartog, G. W. Thurtell, and G. Kidd, "Eddy correlation measurements of methane fluxes using a tunable diode laser at the Kinosheo Lake tower site during the Northern Wetlands Study (NOWES)," *J. Geophys. Res.* **99** (D1), 1511–1517 (1994).
17. R. A. Rooth and N. V. Kema, "Spectroscopic measurements of the  $\nu_2 + 2\nu_3$  band of  $\text{CH}_4$  with a 1.3  $\mu\text{m}$  InGaAsP diode laser," in *Monitoring of Gaseous Pollutants by Tunable Diode Lasers* (Kluwer, Dordrecht, The Netherlands, 1992), pp. 265–273.
18. D. C. Hovde, A. C. Stanton, T. P. Meyers, and D. R. Matt, "Methane emission from a landfill measured by eddy correlation using a fast response diode laser sensor," *J. Atmos. Chem.* **20**, 141–162 (1995).
19. P. Werle, "Laser excess noise and interferometric effects in frequency modulated diode laser spectrometers," *Appl. Phys. B* **60**, 499–506 (1995).
20. P. Werle, R. Mücke, and F. Slemr, "The limits of signal averaging in atmospheric trace gas monitoring by tunable diode laser absorption spectroscopy," *Appl. Phys. B* **57**, 131–139 (1993).
21. P. Werle, B. Scheumann, and J. Schandl, "Real time signal processing concepts for trace gas analysis by TDLAS," *Opt. Eng.* **33**, 3093–3105 (1994).
22. P. Werle and B. Jänker, "High frequency modulation spectroscopy: phase noise and refractive index fluctuations in optical multipass cells," *Opt. Eng.* **35**, 2051–2057 (1996).
23. P. Werle and F. Slemr, "Signal-to-noise ratio analysis in laser absorption spectroscopy using optical multipass cells," *Appl. Opt.* **30**, 430–434 (1991).
24. P. Werle and S. Lechner, "Recent findings and approaches for the suppression of fluctuations and background drifts in tunable diode laser spectroscopy," in *Application of Tunable Diode Lasers and Other Infrared Sources for Atmospheric Studies and Industrial Monitoring*, A. Fried, ed., Proc. SPIE **2834**, 68–78 (1996).
25. J. Faist, F. Capasso, C. Sirtori, D. L. Sivco, J. N. Baillargeon, A. L. Hutchinson, S.-N. G. Chu, and A. Y. Cho, "High power mid-infrared ( $\lambda \approx 5 \mu\text{m}$ ) quantum cascade lasers operating above room temperature," *Appl. Phys. Lett.* **68**, 3680–3682 (1996).
26. R. Q. Yang and S. S. Pei, "Novel type-II quantum cascade lasers," *J. Appl. Phys.* **79**, 8197–8203 (1996).